Available online at www.sciencedirect.com

ScienceDirect

www.elsevier.com/locate/jes

JES JOURNAL OF ENVIRONMENTAL SCIENCES

www.jesc.ac.cn

Effects of phosphate on the transport of graphene oxide nanoparticles in saturated clean and iron oxide-coated sand columns

Jiuyan Chen[1,2], *Weifeng Chen*[3], *Taotao Lu*[4], *Yumeng Song*[1], *Haojing Zhang*[1], *Mengjie Wang*[1], *Xinhai Wang*[1], *Zhichong Qi*[1,2,*], *Minghua Lu*[1,*]

[1] *Henan International Joint Laboratory of Medicinal Plants Utilization, Henan Joint International Research Laboratory of Environmental Pollution Control Materials, Engineering Research Center for Industrial Recirculation Water Treatment of Henan Province, College of Chemistry and Chemical Engineering, Henan University, Kaifeng 475004, China*

[2] *Ministry of Education Key Laboratory of Pollution Processes and Environmental Criteria, Nankai University, Tianjin 300350, China*

[3] *Ministry of Education Key Laboratory of Humid Subtropical Eco-geographical Process, Fujian Provincial Key Laboratory for Plant Eco-physiology, College of Geographical Science, Fujian Normal University, Fujian 350007, China*

[4] *Department of Hydrology, University of Bayreuth, Bayreuth D-95440, Germany*

ARTICLE INFO

Article history:
Received 22 August 2020
Revised 3 October 2020
Accepted 13 October 2020
Available online 1 November 2020

Keywords:
Graphene oxide
Phosphate
Goethite
Transport
Sand

ABSTRACT

In this study, transport behaviors of graphene oxide (GO) in saturated uncoated (i.e., clean sand) and goethite-coated sand porous media were examined as a function of the phosphate. We found that phosphate enhanced the transport of GO over a wide range of solution chemistry (i.e., pH 5.0–9.0 and the presence of 10 mmol/L Na^+ or 0.5 mmol/L Ca^{2+}). The results were mainly ascribed to the increase of electrostatic repulsion between nanoparticles and porous media. Meanwhile, deposition site competition induced by the retained phosphate was another important mechanism leading to promote GO transport. Interestingly, when the phosphate concentration increased from 0.1 to 1.0 mmol/L, the transport-enhancement effect of phosphate in goethite-coated sand was to a much larger extent than that in clean sand. The observations were primarily related to the difference in the total mass of retained phosphate between the iron oxide-coated sand and clean sand columns, which resulted in different degrees of the electrostatic repulsion and competitive effect of phosphate. When the background solution contained 0.5 mmol/L Ca^{2+}, phosphate could be bind to sand/ goethite-coated sand surface by cation bridging; and consequently, promoted competition between phosphate and nanoparticles for deposition sites, which was an important mechanism for the enhanced effect of phosphate. Moreover, the DLVO theory was applicable to describe GO transport behaviors in porous media in the absence or presence of

* Corresponding authors.
E-mails: qizhichong1984@163.com (Z. Qi), mhlu@henu.edu.cn (M. Lu).

https://doi.org/10.1016/j.jes.2020.10.011
1001-0742/© 2020 The Research Center for Eco-Environmental Sciences, Chinese Academy of Sciences. Published by Elsevier B.V.

phosphate. Taken together, these findings highlight the important status and role of phosphate on the transport and fate of colloidal graphene oxide in the subsurface environment.
© 2020 The Research Center for Eco-Environmental Sciences, Chinese Academy of Sciences. Published by Elsevier B.V.

Introduction

As an emerging carbon nanomaterial, graphene oxide (GO) has been applied in numerous applications such as electronics, storage, and optics (Dreyer et al., 2014; Bullo et al., 2019). With the wide production and application increase, GO nanoparticles will inevitably release into groundwater system (Zhao et al., 2014). Moreover, recent studies have shown that GO can be toxic to organisms including bacteria and humans (Chang et al., 2011; Wang et al., 2011a; Jaya Seema et al., 2018). Thus far, findings from recent experimental investigations have established that several chemical conditions (e.g., ionic strength (Feriancikova and Xu, 2012; Qi et al., 2014a, 2014b, 2014c; Dong et al., 2017; Liu et al., 2013; Wang et al., 2017a), pH (Lanphere et al., 2013; Qi et al., 2014b, 2014c), surfactant (Fan et al., 2015a; Wang et al., 2019), divalent cation (Lanphere et al., 2014; Qi et al., 2014b; Fan et al., 2015b; Xia et al., 2015, 2017), organic acid (Chen et al., 2019; Li et al., 2019), and natural organic matter (Qi et al., 2014b, 2014c; Shen et al., 2019)), medium size (Sun et al., 2015; Dong et al., 2016; Chen et al., 2018a), temperature (Wang et al., 2017b, 2019), bacteria (Ramazanpour Esfahani et al., 2020), GO concentration (Sun et al., 2015), and flow rate (Qi et al., 2014b, 2014c; Zhang et al., 2018) had significant influence on the transport behaviors of GO nanoparticles. The results of these investigations confirm that GO exhibits high mobility in subsurface systems under environmentally-relevant solution chemistry conditions. More importantly, GO can serve as a contaminant carrier to significantly enhance the mobility and risks of contaminants (e.g., heavy metal ions and organic contaminants) in porous medium (Qi et al., 2014a; Zhou et al., 2016; Jiang et al., 2018; Sun et al., 2018, 2019; Yin et al., 2019; Zhang et al., 2019; Zhao et al., 2019, 2020). Furthermore, it has been shown that GO could also influence the fate and transport of colloids/biocolloids (e.g., kaolinite, titanium dioxide, hematite, and bacterias) in porous media (Chrysikopoulos et al., 2017; Georgopoulou et al., 2020; Wang et al., 2021; Xia et al., 2019a). However, several other important environmental factors, such as phosphate, have been poorly investigated.

Phosphate is a ubiquitous chemical species in the natural environment including minerals, soils, and water (Wang et al., 2011b; Lei et al., 2016; Xu et al., 2018). In soil solution, particularly in agricultural soil that receives organic fertilizers (e.g., poultry manure and chemical fertilizers), the concentration of phosphate can reach mmol/L levels (Bierman et al., 1995; Wang et al., 2011b; Li and Schuster, 2014; Mu et al., 2017). Particularly, due to possible long period of application of phosphate fertilizers in cropland, a large number of nutrient ions are leached into the groundwater environment (Li and Schuster, 2014; Chen et al., 2015). Previous studies reported that phosphate could influence the surface properties of aquifer media (i.e., soil, clay, and iron oxide) when the phosphate coating bonded to them (Gérard, 2016; Li et al., 2016). Consequently, phosphate possibly affects the environmental behaviors of colloids and contaminants in subsurface environments (Li and Schuster, 2014; Qin et al., 2014). Several studies showed that phosphate could affect the transport of TiO_2 nanoparticles (Chen et al., 2015; Guo et al., 2018; Xu et al., 2018), SiO_2 nanoparticles (Liu et al., 2017), ZnO nanoparticles (Li and Schuster, 2014), and bio-colloids (e.g., bacteria and viruses) (Blanford et al., 2005; Zhuang and Jin, 2008; Wang et al., 2011b) in natural porous media. Hence, considering that phosphate is widely distributed in the soil/water environments (Wang et al., 2011b; Lei et al., 2016; Xu et al., 2018), it may appear as a critical factor in controlling the environmental fate of GO nanoparticles in natural soil/groundwater systems. For example, Ren et al. (2016) found that phosphate enhanced or weakened the effectiveness of Cd^{2+} in destabilizing GO nanoparticles, which depended on the contact order of Cd^{2+}, phosphate, and GO in the natural aqueous solutions. It is necessary to note that the effect of phosphate on the transport of GO may be markedly different from its effect on the transport of other carbon nanoparticles (i.e., carbon nanotubes and fullerene) and metal oxide nanoparticles (i.e., TiO_2 and ZnO) due to the unique physical geometry and surface chemistry of GO (Dreyer et al., 2010). To the best of our knowledge, little is known about the effects of phosphate on the transport properties of GO under various solution chemistry conditions. It is critical, therefore, to study the transport behaviors of GO in the presence of phosphate.

Additionally, the transport of GO in natural groundwater and soil environments is greatly influenced by the interaction between GO and solid matrix (e.g., sand grains, clay minerals, and iron oxides) (Syngouna et al., 2020; Lu et al., 2019). It has been demonstrated that surface charge heterogeneity (e.g., the iron and aluminum oxides) in porous media significantly affected the transport and deposition of GO nanoparticles in granular media due to electrostatic attraction between the positively charged iron oxide and the negatively charged GO nanoparticles as well as increased surface roughness (Duster et al., 2016; Wang et al., 2017a; Chen et al., 2019; Liu et al., 2019; Qi et al., 2019). Moreover, Katzourakis and Chrysikopoulos (2018) reported that surface charge heterogeneity is essential at bench and field scale and cause the solid-matrix surfaces to have spatially variable affinity for colloid attachment (e.g., the spatial variability of collision efficiency) due to the variability in the developed electrostatic forces, consequently affected the transport of colloids. Meanwhile, it is known that phosphate is strongly adsorbed on the oxides of Fe and Al via surface complexation (Tejedor-Tejedor and Anderson, 1990; Persson et al., 1996). It is believed that phosphate may play different roles in GO nanoparticles interaction with porous media containing different degrees of surface charge heterogeneity (e.g., clean sand and iron oxide-

coated sand). Therefore, it is necessary to develop more comprehensive research to understand the different attachment behavior of GO onto various iron oxide minerals.

The primary objective of this work was to explore the influence of phosphate on GO transport in uncoated (i.e., clean sand) and iron oxide-coated sand (using goethite as the model iron oxides) columns. Column experiments of GO were conducted in the presence of Na^+ or Ca^{2+}; meanwhile, the effects of phosphate on the transport of GO at different pH were also investigated. The specific goals are to identify the differences in transport properties of GO in saturated clean sand and goethite-coated sand as affected by phosphate. Moreover, to understand phosphate coating on porous medium effects on GO transport, we conducted additional experiments by first saturating the sand with phosphate solution before injecting GO suspension through the columns. The different mechanisms by which phosphate affects the transport behavior of GO in uncoated and goethite-coated sand porous media were discussed. Meanwhile, the Derjaguin-Landau-Verwey-Overbeek (DLVO) theory was applied to gain further insights into the effects of phosphate.

1. Materials and methods

1.1. Materials

GO sheets (purity: >99%) were provided by Plan Nano Materials Tech Co. (Tianjin, China). The important physicochemical properties of the product were described in our previous study (Li et al., 2019). Briefly, the specific surface area of the GO (207.1 m^2/g) based on the Brunauer–Emmer–Teller method was determined by an ASAP 2020 surface area analyzer (Micromeritics, GA, USA); the product contained 62.1% C, 34.2% O, and small amounts of H and N (measured by an elemental analyzer (Vario EL, Elementar Analysensysteme, Germany). The surface functional groups were mainly hydroxyl, carboxyl, and carbonyl groups.

Quartz sand was purchased from Sigma–Aldrich (St. Louis, MO) (purity >99.9%, 0.21–0.30 mm, and 0.26 mm average grain size). Before use, the sand grains were cleaned by 0.1 mol/L hydrochloric acid and 5% hydrogen peroxide to effectively remove impurities on the sand surface according to the method described in our previous study (Li et al., 2019).

The method for the preparation of goethite-coated sand is reported in the literature (Stahl and James, 1991). The detailed preparation procedures are available in Appendix A Section S1. The ζ-potential of porous media was determined by Zeta-Plus potential analyzer (Zetasizer nano ZS90, Malvern Instruments, UK) (Mitropoulou et al., 2013; Chrysikopoulos et al., 2017). Details of the method are given in Appendix A Section S2.

1.2. Preparation and characterization of GO nanoparticles

The GO stock suspension (300 mg/L) was prepared by adding 300 mg GO into 1 L deionized water (DI water). Then, the mixture was ultrasonically dispersed in the water bath at 500 W for 4 hr. The ζ-potential and hydrodynamic diameter (Z_{avg}) of GO under the test conditions were measured by dynamic light scattering (DLS) measurements using a Zeta-Plus potential analyzer described above.

Before initiating the column experiments, the influents (containing 10 mg/L of GO) were prepared temporarily by diluting the stock GO suspension and phosphate stock solution within the electrolyte solutions to obtain the desired solution (Table 1). Additionally, each desired pH value of the GO suspensions (with or without phosphate) was achieved by 0.1 mol/L HCl or NaOH.

1.3. Column transport experiments

Clean sand (i.e., treaded sand) or goethite-coated sand was dry-packed into columns made up of borosilicate glass (10 cm length and 11 mm inner diameter). Each column contained approximately 15 g sand with an average bulk density of 1.55 ± 0.01 g/cm^3, and an average porosity of 0.41 ± 0.01. The columns were operated in an upward direction at a constant pore velocity of 0.31 cm/min using syringe pumps (KD Scientific, Holliston, MA). Firstly, the column was flushed with 13 pore volumes (PV) of DI water to establish a steady-state flow condition, and then equilibrated with the background electrolyte solution (~21 PV). Then, 21 PV of GO nanoparticle suspension (in the absence or presence of phosphate) was injected into the sand column. Finally, the column was eluted with 6 PV of GO-free background solution. In selected experiments (columns 9–10 and 17–18, Table 1), the columns were first saturated the porous medium with 13 PV of phosphate solution (0.5 mmol/L) before flushing GO suspension through the column, and then 21 PV of GO nanoparticle suspension (without phosphate) was injected into the sand column. It is noteworthy that phosphate did not result in the dissociation of goethite from the sand grains (even at low pH conditions) (**Appendix A Fig. S1**). The effluents were collected every 3.5 PV, and the concentrations of GO in the influent (C_0_GO) and effluent (C_GO) were measured by using a UV–vis spectrophotometer (PuXi Analytical Instrument Co. Ltd, Beijing, China) at 230 nm in order to obtain the breakthrough curves (Wang et al., 2009). Then the effluents were centrifuged (15,000 r/min) for 20 min by high-speed centrifuge (sigma 3–18k, Germany) and the supernatants were withdrawn. The concentration of phosphate in the supernatant was analyzed using the molybdenum blue method (Liu and Chen, 2016). The details for the method are provided in **Appendix A** Section S3. Note that under the test conditions of this study the phosphate concentration in the effluent (C_phosphate) and in supernatant (C_e_phosphate) are essentially equal (for example, the mass of phosphate in the adsorbed phase (i.e., adsorbed by GO) was typically less than 0.3 to 2% of the total mass of phosphate in the system, **Appendix A Fig. S2**). Previous studies also confirmed that adsorption affinities of GO nanoparticles for phosphate were very weak (Ren et al., 2016; Xu et al., 2016a). Finally, retention profiles of GO and phosphate were obtained after transport experiments (the detailed procedures are given in **Appendix A** Section S4). The mass balances of GO nanoparticles and phosphate in the column experiments were within the range of 91.0 to 99.8% and 92.9 to 99.9%, respectively (**Appendix A Tables S1 and S2**). Furthermore, the total mass of retained phosphate in column was calculated based on a mass balance approach (i.e., retained mass = influ-

Table 1 – Selected properties of GO suspensions and porous media under different solution chemistry conditions.

Column No.	porous media	Background solution	pH	ζ-potential of GO[a] (mV)	ζ-potential of porous medium[b] (mV)	$Z_{ave\text{-}GO}$ [c] (nm)
1	sand	10 mmol/L NaCl	5.0	−30.3 ± 1.6	−20.1 ± 1.4	256.9 ± 1.8
2	sand	10 mmol/L NaCl + 0.1 mmol/L phosphate	5.0	−30.8 ± 0.8	−22.7 ± 0.5	228.6 ± 3.9
3	sand	10 mmol/L NaCl + 0.5 mmol/L phosphate	5.0	−31.9 ± 0.2	−23.8 ± 2.3	213.9 ± 10.6
4	sand	10 mmol/L NaCl + 1.0 mmol/L phosphate	5.0	−32.5 ± 1.7	−25.3 ± 1.5	205.7 ± 9.2
5	goethite-coated sand	10 mmol/L NaCl	5.0	−30.3 ± 1.6	−10.2 ± 1.3	236.9 ± 1.8
6	goethite-coated sand	10 mmol/L NaCl + 0.1 mmol/L phosphate	5.0	−30.8 ± 0.8	−12.6 ± 1.4	228.6 ± 3.9
7	goethite-coated sand	10 mmol/L NaCl + 0.5 mmol/L phosphate	5.0	−31.9 ± 0.2	−17.4 ± 1.0	256.9 ± 1.8
8	goethite-coated sand	10 mmol/L NaCl + 1.0 mmol/L phosphate	5.0	−32.5 ± 1.7	−21.7 ± 2.1	205.7 ± 9.2
9 [d]	sand	10 mmol/L NaCl, phosphate-saturated column	5.0	−30.3 ± 1.6	−23.8 ± 2.3	256.9 ± 1.8
10 [d]	goethite-coated sand	10 mmol/L NaCl, phosphate-saturated column	5.0	−30.3 ± 1.6	−18.4 ± 1.9	256.9 ± 1.8
11	sand	0.5 mmol/L $CaCl_2$	5.0	−17.2 ± 1.4	−16.9 ± 1.7	537.3 ± 22.6
12	sand	0.5 mmol/L $CaCl_2$ + 0.1 mmol/L phosphate	5.0	−18.1 ± 2.1	−18.4 ± 1.1	454.6 ± 12.7
13	sand	0.5 mmol/L $CaCl_2$ + 0.5 mmol/L phosphate	5.0	−18.3 ± 1.6	−23.4 ± 1.1	351.3 ± 18.9
14	goethite-coated sand	0.5 mmol/L $CaCl_2$	5.0	−17.2 ± 1.4	−8.5 ± 1.0	537.3 ± 22.6
15	goethite-coated sand	0.5 mmol/L $CaCl_2$ + 0.1 mmol/L phosphate	5.0	−18.1 ± 2.1	−11.4 ± 1.7	454.6 ± 12.7
16	goethite-coated sand	0.5 mmol/L $CaCl_2$ + 0.5 mmol/L phosphate	5.0	−18.3 ± 1.6	−19.7 ± 2.6	351.3 ± 18.9
17 [d]	sand	0.5 mmol/L $CaCl_2$, phosphate-saturated column	5.0	−17.2 ± 1.4	−23.4 ± 1.1	537.3 ± 22.6
18 [d]	goethite-coated sand	0.5 mmol/L $CaCl_2$, phosphate-saturated column	5.0	−17.2 ± 1.4	−19.7 ± 2.6	537.3 ± 22.6
19	sand	10 mmol/L NaCl	7.0	−31.5 ± 2.0	−24.0 ± 1.2	223.5 ± 9.7
20	sand	10 mmol/L NaCl + 0.5 mmol/L phosphate	7.0	−32.3 ± 1.3	−27.8 ± 0.9	218.7 ± 12.5
21	sand	10 mmol/L NaCl	9.0	−33.7 ± 2.5	−26.3 ± 1.5	230.8 ± 11.2
22	sand	10 mmol/L NaCl + 0.5 mmol/L phosphate	9.0	−35.2 ± 1.3	−31.7 ± 2.2	226.8 ± 7.9
23	goethite-coated sand	10 mmol/L NaCl	7.0	−31.5 ± 2.0	−15.9 ± 0.5	223.5 ± 9.7
24	goethite-coated sand	10 mmol/L NaCl + 0.5 mmol/L phosphate	7.0	−32.3 ± 1.3	−22.5 ± 2.2	218.7 ± 12.5
25	goethite-coated sand	10 mmol/L NaCl	9.0	−33.7 ± 2.5	−21.6 ± 0.9	230.8 ± 11.2
26	goethite-coated sand	10 mmol/L NaCl + 0.5 mmol/L phosphate	9.0	−35.2 ± 1.3	−25.9 ± 0.6	226.8 ± 7.9

[a] Zeta potential of GO; values after ± sign represent standard deviation of five replicates.
[b] Zeta potential of quartz sand; values after ± sign represent standard deviation of five replicates.
[c] Hydrodynamic diameter of GO based on DLS analysis; values after ± sign represent standard deviation of three replicates.
[d] Column was presaturated with phosphate before injecting GO suspension.

ent mass – effluent mass – eluted mass. Note that the effluent mass represent the mass of phosphate in the effluent samples when GO nanoparticle suspension with phosphate was injected into the sand column, the eluted mass represent the mass of phosphate in the effluent samples when the column was eluted with GO-free background solution.).

1.4. *Batch sorption experiments*

A batch sorption method was conducted to investigate the binding affinities of phosphate onto GO nanoparticles and porous media (i.e., clean sand and goethite-coated sand) under various solution chemistry conditions. The detailed adsorption procedures are present in **Appendix A** Sections S3 and S5.

1.5. *DLVO theory*

DLVO theory has commonly been applied to qualitatively explain the transport of colloid in porous media (Wang et al., 2017a). The total interaction energy (V_{TOT}) was determined as the sum of van der Waals (V_{VDW}) attraction and electrostatic repulsion (V_{EDL}). The detailed description regarding the equations is provided in **Appendix A** Section S6.

2. Results and discussion

2.1. *Transport of GO nanoparticles as affected by phosphate*

The effects of different phosphate concentrations on the transport of GO in clean sand and goethite-coated sand columns are illustrated in **Fig. 1**. The retention profiles are provided in Appendix A **Fig. S3**. Because the value of pH_{PZC} (point of zero charge) is 7.8 to 9.3 for goethite (Kosmulski, 2004), goethite has positive charges on the surface under the experimental condition (i.e., pH 5.0). In the absence of phosphate, goethite coating inhibited the transport of GO mainly due to the increase of electrostatic attraction between nanoparticles and porous media (**Appendix A Fig. S4**) (Duster et al., 2016; Wang et al., 2017a; Chen et al., 2019; Qi et al., 2019). Meanwhile, compared with clean sand, the high roughness of goethite-coated sand surface also caused GO nanoparticles to deposit more easily (Morales et al., 2009; Shen et al., 2011). Previous studies have confirmed that surface roughness had a significant effect on the retention of colloids in porous media, e.g., rougher surfaces clearly retained more colloids than smooth ones (Morales et al., 2009). Moreover, the DLVO interaction energies between GO and sand/goethite-coated sand was calculated, and the maximum energy bar-

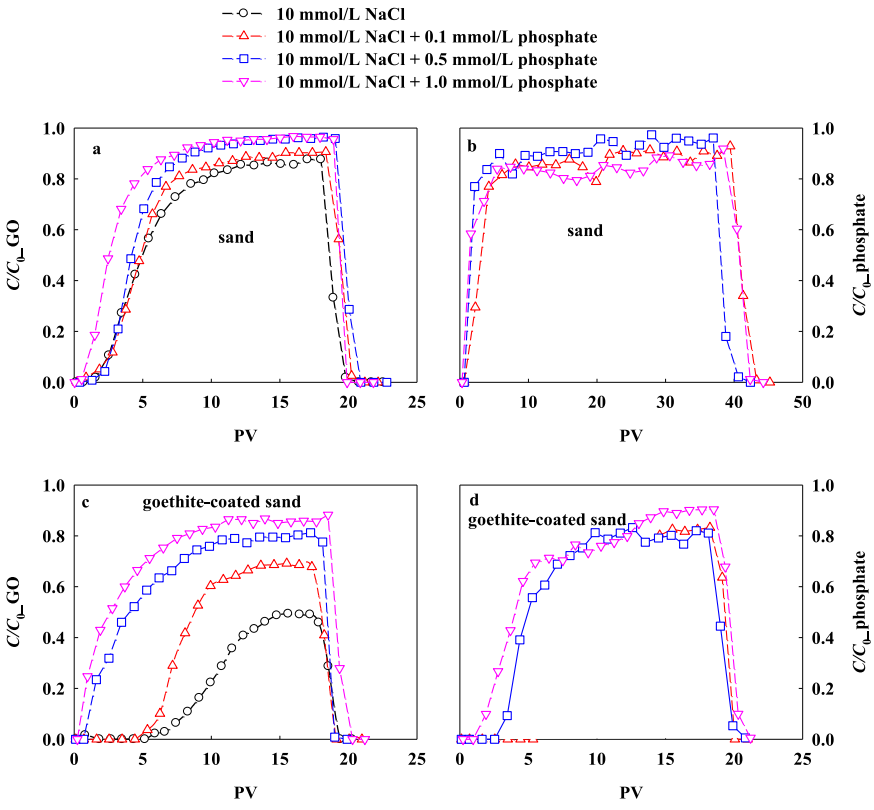

Fig. 1 – Effects of phosphate on the transport of GO nanoparticles (10 mg/L at pH 5.0) in quartz sand (columns 1–4) and goethite-coated sand (columns 5–8) at 10 mmol/L NaCl. (a) and (c) the breakthrough curves of GO in each of the experiments; (b) and (d) the breakthrough curves of phosphate in the respective experiments.

rier (Φ_{max}) and the secondary energy minimum (Φ_{sec}) are provided in **Appendix A Table S3**. The results indicated that the surface heterogeneity of sand grains had significant effect on the hight of Φ_{max} depth of Φ_{sec} for GO (**Appendix A Fig. S5**) (Wang et al., 2012a). While the presence of the high Φ_{max} (55.5 K_BT and 22.1 K_BT in sand and goethite-coated sand, respectively) would inhibit GO deposition at the primary energy minimum well, the GO could be immobilized at the secondary minimum energy well (Fan et al., 2015b; Lucia and Xu, 2012; Xia et al., 2019b). However, the secondary minimum energy well of GO in the goethite-coated sand column was shallower than that in the sand column (–0.52 K_BT vs. –0.11 K_BT subgraph in **Appendix A Fig. S5**), indicating that the contribution of the secondary minimum was less significant in geochemically heterogeneous porous media (i.e., goethite-coated sand) than clean sand (Wang et al., 2017a). On the basis of the fact that presence of goethite coating suppressed GO transport (**Appendix A Fig. S4**), we propose that goethite (positively charged) created a favorable condition the deposition of GO nanoparticles (negatively charged) (Feng et al., 2019); and consequently, the nanoparticles were primarily trapped in the primary minimum rather than secondary minimum (Wang et al., 2017a).

Interestingly, when phosphate was added into the influents, phosphate enhanced GO transport in both porous media under the experimental condition (10 mmol/L NaCl, pH 5.0), and became more significant with increasing phosphate concentration. For instance, in the absence of phosphate, the maximum C/C_0 of GO reached 85% and 49% in clean sand and goethite- coated sand, respectively. Whereas, in the presence of 0.5 mmol/L phosphate, the values increased to 96% and 85% in sand and goethite-coated sand columns, respectively. Phosphate facilitated GO transport based on three mechanisms. Firstly, even though phosphate has slight effect on the ζ-potential of GO (**Appendix A Fig. S6a**), phosphate can greatly influence the surface properties of sand and iron oxides when it binds to them (Wang et al., 2011b; Tofan-Lazar and Al-Abadleh, 2012; Wang et al., 2016). Previous studies have confirmed that the charge of the grain surface could be modified from positive to negative due to the adsorbed phosphate ions (Park et al., 2009). As shown in **Table 1** and **Appendix A Fig. S6a**, phosphate increased the negative charge of the porous media. The increase in electrostatic repulsion between the nanoparticles and sand grains promoted GO transport (Lanphere et al., 2013; Wang et al., 2017a), thereby inhibited the deposition of GO at the secondary minimum energy well (Tufenkji and Elimelech, 2004, 2005). Secondly, Phosphate had a high affinity for the grain surfaces, resulting in decreasing the deposition of nanoparticles (Weng et al., 2008; Qin et al., 2012). Thus, competition between phosphate ions and GO nanoparticles for the fewer deposition sites on porous media surfaces contributed to promote the transport of GO (as evidence by both breakthrough curves and retention profiles of phosphate (**Fig. 1, Appendix A Figs. S3c**, and **S3d**)) (Han et al., 2013; Ren et al.,

2016; Xu et al., 2018). Thirdly, phosphate could inhibit the aggregation of GO nanoparticles (Table 1 and Appendix A Fig. S6b). Note that phosphate slightly affected the hydrodynamic particle sizes (e.g., the average hydrodynamic diameter of GO decreased from 256.9 nm (in the absence of phosphate) to 205.7 nm (in the presence of 0.5 mmol/L phosphate)); thus, the decrease of GO particle sizes likely played insignificant role in GO transport (Li et al., 2019). Additionally, in the absence of phosphate, the retention profiles of GO in goethite-coated sand column exhibited hyperexponential distribution in shape (Appendix A Fig. S3b), which was ascribed to the physical and chemical heterogeneity of the porous media surface (Tufenkji and Elimelech, 2005; Dengjun Wang, 2012; Leij et al., 2016). Similar results were also identified in previous studies (Wang et al., 2017a; Chen et al., 2019). Hyperexponential profiles of retained GO tended to become exponential in shape in the presence of phosphate. This was probably because the presented phosphate masked the heterogeneity of the grain surface. Similarly, previous studies demonstrated that the retention profiles of retained colloids evolved exponential in the addition of dissolved organic matter (e.g., humic acid) (Lecoanet et al., 2004; Liang et al., 2013). Calculations based upon DLVO theory suggested that the interaction energy profiles were sensitive to the changes of phosphate concentration. For clean sand, the Φ_{max} values increased from 55.5 K_BT (without phosphate) to 61.2 K_BT (with 0.1 mmol/L phosphate) and then to 70.6 K_BT (with 1.0 mmol/L phosphate) (Appendix A Fig. S7a and Table S3). The large energy barriers in the presence of high phosphate concentration indicated that GO was difficult to deposit in the primary energy minimum on the surfaces of sand grains (Fan et al., 2015b; Sun et al., 2015; Wang et al., 2017a). Accordingly, the Φ_{sec} values decreased from –0.52 K_BT (without phosphate) to –0.37 K_BT (with 1.0 mmol/L phosphate) (Appendix A Table S3), indicating that the increase of electrostatic repulsion inhibited the deposition of GO at the secondary minimum energy well (Tufenkji and Elimelech, 2004, 2005). The goethite-coated sand columns exhibited the same result (Appendix A Fig. S7b and Table S3).

Intriguingly, with increasing phosphate concentration (from 0 to 1 mmol/L), the transport-enhancement effect of phosphate in goethite-coated sand was to a much larger extent than that in clean sand. As shown in Fig. 1, the maximum C/C_0 values of GO slowly increased from 85% (in the absence of phosphate) to 90% (0.1 mmol/L phosphate) to 94% (0.3 mmol/L phosphate) and then to 96% (0.5 mmol/L phosphate) in clean sand columns. In comparison, the maximum C/C_0 values of GO sharply increased from 49% (in the absence of phosphate) to 68% (0.1 mmol/L phosphate) to 79% (0.3 mmol/L phosphate) and then to 86% (0.5 mmol/L phosphate) in goethite-coated sand columns. Meanwhile, this observation is in line with the different trends of values of Φ_{max} and Φ_{sec} in Appendix A Table. S3. The observation suggested that the extent of the enhancement effects of phosphate on GO transport were varied considerably depending on the physicochemical characteristics of the porous media (e.g., homogeneity and heterogeneity). On the one hand, as mentioned above, the electrostatic repulsion was an important mechanism for the transport-enhancement effect of phosphate (Han et al., 2013; Li and Schuster, 2014; Xu et al., 2018). The difference of ζ-potential

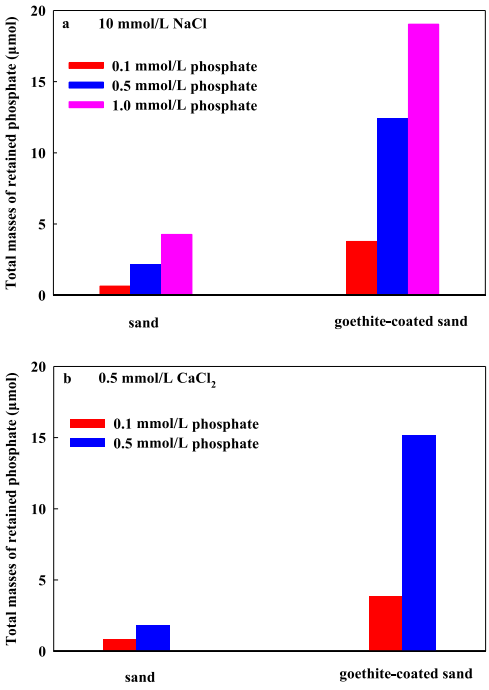

Fig. 2 – The total masses of retained phosphate in sand columns and goethite-coated sand columns: (a) at 10 mmol/L NaCl (columns 2 – 4 and 6 – 8) and (b) at 0.5 mmol/L $CaCl_2$ (columns 12–13 and 15–16). The total mass of retained phosphate in column = influent mass – effluent mass–eluted mass.

values of goethite-coated sand grains with various phosphate concentrations (–12.6, –17.4, and –21.7 mV in the presence of 0.1, 0.5, and 1.0 mmol/L phosphate, respectively) were greater than those of sand grains (–22.7, –23.8, and –25.3 mV in the presence of 0.1, 0.5, and 1.0 mmol/L phosphate, respectively) (Table 1). In this case, the differences in the extent of the electrostatic repulsion between goethite-coated sand grains and GO nanoparticles with various phosphate concentrations were larger than those between sand grains and GO. Consequently, the difference of electrostatic repulsion affected the extent of enhancement effect of phosphate in sand and goethite-coated sand. On the other hand, and more importantly, it has been reported that phosphate ions could form hydrogen-bonded complexes and inner-sphere complexes (i.e., mono-, and polynuclear complexes) on the silica surface and goethite surface, respectively (Murashov et al., 1999; Nowack and Stone, 2006; Xu et al., 2016b). Consequently, the binding affinity of phosphate to sand surfaces was much weaker than that to goethite-coated sand surfaces (see the adsorption coefficients (K_d) of phosphate to clean sand and goethite-coated sand in Appendix A Fig. S8). Additionally, on the base of the breakthrough curves of phosphate, the difference of calculated total masses of retained phosphate with different initial phosphate concentrations in goethite-coated sand columns was also greater than those in sand columns (Fig. 2). Therefore, competitive effect of phosphate on goethite-coated sand surfaces was stronger than on sand surfaces. Consequently, the enhancement effect of phosphate

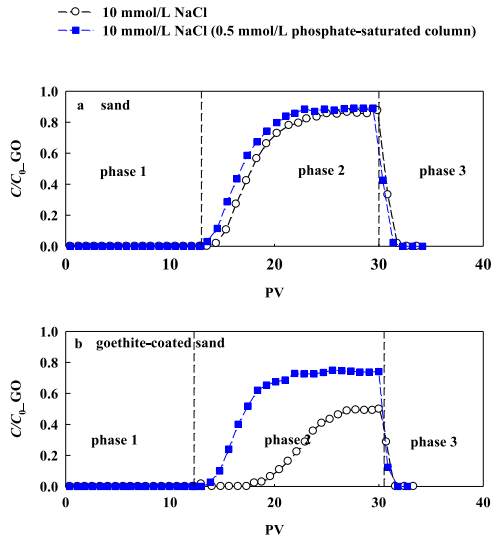

Fig. 3 – Effects of phosphate coating on porous medium on the transport of GO (10 mg/L at pH 5.0) in (a) quartz sand (columns 3 and 9) and (b) goethite-coated sand (columns 7 and 10) at 10 mmol/L NaCl (pH 5.0). The columns were saturated with 0.5 mmol/L phosphate in phase 1, GO transport at 10 mmol/L NaCl in phase 2; the columns were eluted with 10 mmol/L NaCl in phase 3.

on GO transport in goethite-coated sand was to a larger extent than that in sand when phosphate concentration increased from 0.1 to 1.0 mmol/L. Moreover, GO without phosphate exhibited higher mobility in clean sand than that in goethite-coated sand (Appendix A **Fig. S4**), so this might be another reason that caused the enhancement in clean sand was relatively smaller in the presence of phosphate.

Furthermore, in order to clarify the role of the adsorbed phosphate on clean sand and goethite-coated sand in GO transport, the porous media was saturated using the phosphate solutions (0.5 mmol/L) before injecting GO suspensions through the column (Fig. 3) (Yang et al., 2012; Xia et al., 2015; Zhang et al., 2020), and the breakthrough curves of phosphate and retention profiles are provided in Appendix A **Fig. S9** and **Fig. S10**, respectively. In this case, both the clean sand and goethite-coated sand were bound with phosphate, which slightly facilitated the transport of GO in the columns saturated with phosphate solutions comparing with the transport of GO without phosphate (the maximum C/C_0 values of GO gradually increased from 85% to 88%) (Fig. 3a). Whereas, in the goethite-coated sand, GO transport in the phosphate-saturated sand column was considerably enhanced in comparison with the transport of GO without phosphate—not only was the maximum C/C_0 value of GO reached more quickly, but the value sharply increased from 49% to 75% (Fig. 3b). These results are consistent with the mechanisms mentioned

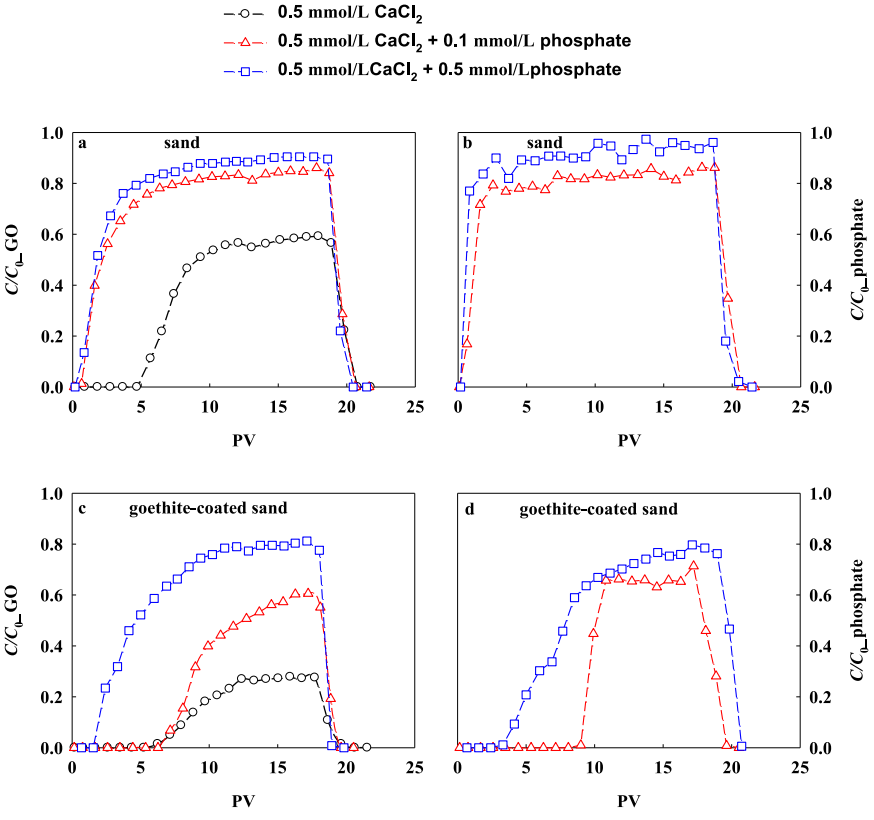

Fig. 4 – Effects of phosphate on the transport of GO (10 mg/L at pH 5.0) in quartz sand (columns 11–13) and goethite-coated sand (columns 14–16) at 0.5 mmol/L $CaCl_2$.
(a) and (c) the breakthrough curves of GO in each of the experiments; (b) and (d) the breakthrough curves of phosphate in the respective experiments.

above. That is, the transport-enhancement effect of phosphate (via the increase of electrostatic repulsion and deposition site competition induced by the retained phosphate) in goethite-coated sand was to a much larger extent than did in sand.

2.2. *Effects of phosphate on the transport of GO nanoparticles in the presence of Ca^{2+}*

The effects of phosphate on GO transport in saturated clean sand and goethite-coated sand in the presence of Ca^{2+}were investigated (Fig. 4). The retention profiles are given in Appendix A **Fig. S11**. Similarly, both in sand and goethite-coated sand columns, phosphate also enhanced GO transport. For example, the maximum C/C_0 of GO increased from 58% and 27% (in the absence of phosphate) to 85% and 57% (with 0.1 mmol/L phosphate) to 90% and 80% (with 0.5 mmol/L phosphate) in the clean sand and goethite-coated sand columns, respectively. On the basis of interpretation mentioned above, phosphate could change the surface charge of sand/goethite-coated sand grains when it was adsorbed onto them. For clean sand, the divalent metal cation enhanced the adsorption of phosphate by forming sand–Ca–phosphate complexs, the dominant mechanism was cation bridging (i.e., dissolved Ca^{2+}ions served as a bridging agent between phosphate and sand grains) (Fan et al., 2015b; Xia et al., 2015). For goethite-coated sand, free Ca^{2+} ions could not readily bind to the iron oxide surface due to the electrostatic repulsion (Zhang et al., 2018). However, as mention above, phosphate ions could form ≡Fe–phosphate complexes (Nowack and Stone, 2006; Xu et al., 2016b). In this case, Ca^{2+} was possibly captured by the preloaded phosphate, and consequently further enhanced phosphate sequestration by the formation of multiple ≡Fe −phosphate−Ca−phosphate complexes (Zhang et al., 2018). Therefore, the presence of phosphate increased the electrostatic repulsion between GO and porous media (i.e., sand and goethite-coated sand) in the addition of Ca^{2+} (as evidenced by the ζ-potential values of GO and porous media with or without phosphate, Table 1 and Appendix A **Fig. S6c**) (Wang et al., 2017a; Qi et al., 2019). Meanwhile, the deposited phosphate ions on the grain surfaces could compete with GO nanoparticles for deposition sites (also proved by the breakthrough and retention of phosphate in the **Fig. 4**, Appendix A **Figs. S8c**, and **S8d**) (Han et al., 2013; Xu et al., 2018), resulting in enhancing the transport of GO. In addition, compared with Na^+, phosphate was more effective in inhibiting aggregation of GO nanoparticles in the presence of Ca^{2+} (for example, the Z_{avg} values of GO decreased from 537.3 nm (without phosphate) to 351.3 nm (with 0.5 mmol/L phosphate), Table 1 and Appendix A **Fig. S6b**); therefore, the decrease of GO particle sizes likely played significant role in enhancing GO transport in the presence of Ca^{2+}(Lanphere et al., 2013; Qi et al., 2014b; Fan et al., 2015b). Furthermore, this trend was qualitatively in line with the DLVO interaction energy profiles (i.e., the maximum energy barrier (Φ_{max}) became higher as the phosphate concentration increased (Appendix A **Fig. S12**).

When the phosphate concentration increased from 0.1 to 0.5 mmol/L, a surprising observation was that the transport-enhancement effect of phosphate in sand (e.g., the C/C_0 value increased from 85% and 90%, Fig. 4**a**) was to a much weaker extent than that in goethite-coated sand (e.g., the C/C_0 value increased from 57% and 80%, Fig. 4**b**). This observation could possibly be explained by two major mechanisms. Firstly, the difference of ζ-potential values of goethite-coated sand grains between presence of 0.1 mmol/L and 0.5 mmol/L phosphate (–8.5 vs. –19.7 mV) were greater than those of sand grains (–16.9 vs. –23.4 mV). In other words, the differences in the extent of the electrostatic repulsion between porous media and GO were contributed to the difference of transport-enhancement effect. Secondly, as discussed earlier, competition between GO and phosphate for the deposition sites was another essential mechanism for transport-enhancement effect of phosphate (Han et al., 2013; Xu et al., 2018). As shown in Fig. 2b and Appendix A **Table S2**, the total mass of retained phosphate (in the presence of 0.5 mmol/L) was about one time more than that in the presence of 0.1 mmol/L phosphate in sand columns (i.e., 1.78 vs.0.86 μmol). In comparison, in goethite-coated sand columns, the total mass of retained phosphate (the initial phosphate concentration was 0.5 mmol/L) was about four times higher than that in the presence of 0.1 mmol/L phosphate (i.e., 3.8 vs.15.2 μmol). In this case, competitive effect of phosphate on sand surfaces was weaker than on goethite-coated sand surfaces. Hence, phosphate enhanced GO transport in goethite-coated sand to a larger extent than did in sand when phosphate concentration increased from 0.1 to 0.5 mmol/L.

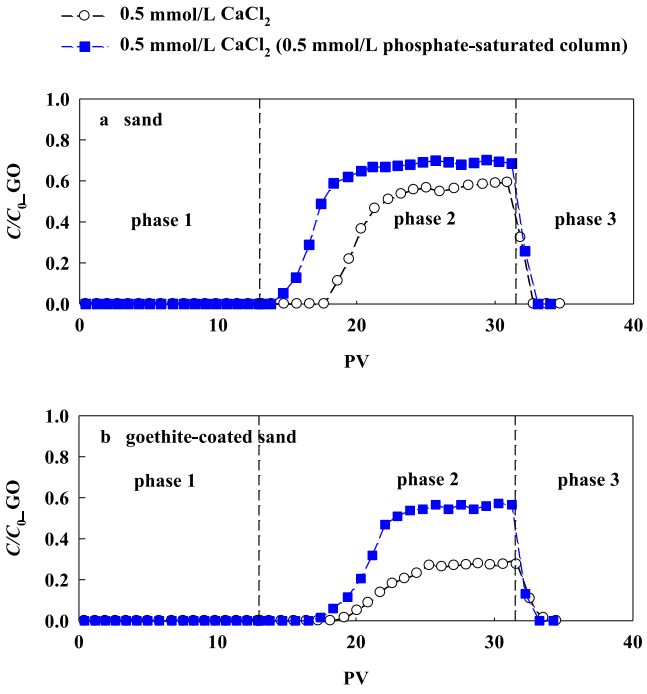

Fig. 5 – Effects of phosphate coating on porous medium on the transport of GO (10 mg/L at pH 5.0) in (a) quartz sand (columns 13 and 17) and (b) goethite-coated sand (columns 16 and 18) at 0.5 mmol/L $CaCl_2$ (pH 5.0). The columns were saturated with 0.5 mmol/Lphosphate in phase 1, GO transport at 0.5 mmol/L $CaCl_2$ in phase 2; the columns were eluted with 0.5 mmol/L $CaCl_2$ in phase 3.

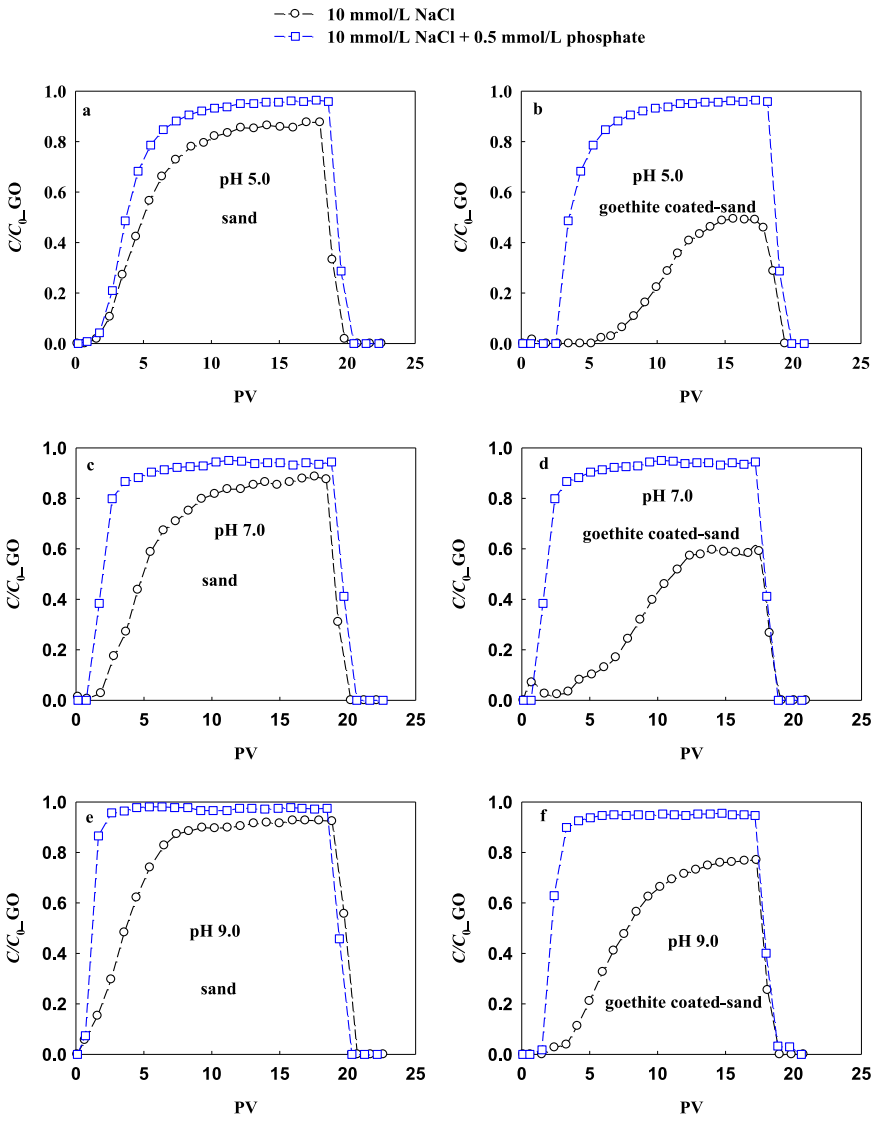

Fig. 6 – Effects of phosphate (0.5 mmol/L) on transport of GO (10 mg/ L) in quartz sand (a, c, and e, columns 1, 3, 19–22) in goethite-coated sand (b, d, and f, columns 5, 7, 23–26) under different pH conditions.

Furthermore, we also conducted additional experiments by saturating the porous media with the phosphate solutions (0.5 mmol/L) before injecting GO suspensions through the column (Fig. 5). The breakthrough curves of phosphate and retention profiles are given in Appendix A **Fig. S13** and **Fig. S14**, respectively. Interestingly, unlike Na^+, the transport of GO in the phosphate-saturated sand column was considerably enhanced in comparison with the transport of GO without phosphate (the maximum C/C_0 values of GO increased from 58% to 70%) (Fig. 5a). This observation is consistent with the mechanisms discussed earlier. Sand grains exhibited much higher adsorption capacities for phosphate in the presence of Ca^{2+} than in the presence of Na^+ due to the cation bridging (Appendix A **Fig. S5**) (Millero et al., 2001; Rietra et al., 2001; Lin et al., 2017).Thus, the phosphate coating in the presence of Ca^{2+} enhanced GO transport more significantly than did in the presence of Na^+ due to the more significant competitive effect of adsorbed phosphate.

2.3. *Effects of phosphate on the transport of GO nanoparticles under different pH conditions*

The effects of phosphate on GO transport in uncoated and goethite-coated sand under different pH conditions (5.0, 7.0, and 9.0) are also investigated (Fig. 6). The retention profiles are present in Appendix A **Fig. S15**.The results showed that phosphate could facilitate GO transport under all the tested pH. Note that phosphate has a slight effect on the ζ-potential of GO over the pH range from 5.0 to 9.0 (Table 1). Thus, as mentioned above, the main mechanisms of enhanced GO transport by phosphate were ascribed to the enhanced electrostatic repulsion between porous media and GO nanoparticles, and the competition between GO nanoparticles and phosphate ions for deposition sites (Han et al., 2013; Ren et al., 2016; Chen et al., 2018b; Xu et al., 2018). It is noted that the deposition of phosphate on the grain surfaces decreases with increasing pH from 5.0 to 9.0 due to the increase of electrostatic

repulsion between phosphate ions and porous media (note that dominant species of phosphate changed from H_2PO- 4 (at pH 5.0) to HPO2- 4 at pH 9.0 (Stumm and Morgan, 1981; Tejedor-Tejedor and Anderson, 1990); this is evident by the transport and deposition of phosphate in **Appendix A Figs. S16** and **S17**. Consequently, the competitive effect of phosphate ions decreased with increasing solution pH.

Interestingly, at a given pH value, the transport-enhancement effect of phosphate in goethite-coated sand was to a much larger extent than that in sand. For instance, the value of maximum C/C_0 of GO increased from 92% (without phosphate) and 95% (with 0.5 mmol/L phosphate) in sand columns at pH 9.0 (Fig. 6e); in comparison, the maximum C/C_0 of GO increased from 76% to 93% in goethite-coated sand columns (Fig. 6f). Meanwhile, this observation is in line with the trends of the DLVO interaction energy profiles (**Appendix A Fig. S18**). Goethite-coated sand had a much larger phosphate sorption capacity than sand grains under the same pH condition (**Fig. 9**). Thus, more phosphate ions competed with nanoparticles for deposition sites in the goethite-coated sand columns, which could be more effective in enhancing the transport of GO (Han et al., 2013; Xu et al., 2018). The results further highlight the roles of retained phosphate in the transport-enhancement effect of phosphate during the transport process.

3. Conclusions

The present study clearly demonstrates phosphate has enhanced effects on GO transport in saturated uncoated and iron oxide-coated sand columns. The transport–enhancement effect of phosphate was attributed to the increase of electrostatic repulsion between porous media and nanoparticles as well as deposition site competition induced by the retained phosphate. Interestingly, when the concentration of phosphate increased from 0.1 to 1.0 mmol/L, the enhancement effect of phosphate on GO transport in goethite-coated sand was to a larger extent than that in clean sand, mainly because the differences in the extent of the electrostatic repulsion as well as the competitive effect of retained phosphate in goethite-coated sand columns were larger than those in sand columns. Furthermore, when the background solution contained 0.5 mmol/L Ca^{2+}, phosphate could bind to clean sand/goethite-coated sand through cation bridging, resulting in facilitating the transport of GO. Also, the DLVO theory were applicable to interpret the phosphate-dependent transport of GO. Overall, the findings of the present study will improve the current understanding of the environmental behaviors of GO in natural soil/groundwater systems containing phosphate, which can influence the transport of GO.

Acknowledgments

This work was supported by the National Natural Science Foundation of China (No. 21707081), the Opening Foundation of Ministry of Education Key Laboratory of Pollution Processes and Environmental Criteria (No. 2018-06), Science and Technology Major Project of Henan Province, Henan, China (No. CX0001F01800), the College Students' Innovative Training Program of Henan Province (No. 202013501013), the Project Management of Innovation and Entrepreneurship Training Program for Minsheng College Students (No. MSCXSY2019013), and the China Scholarship Council (No. 201708420145).

Appendix A Supplementary data

Supplementary material associated with this article can be found, in the online version, at doi:10.1016/j.jes.2020.10.011.

REFERENCES

Bierman, P.M., Rosen, C.J., Bloom, P.R., Nater, E.A., 1995. Soil solution chemistry of sewage-sludge incinerator ash and phosphate fertilizer amended soil. J. Environ. Qual. 24, 279–285.

Blanford, W.J., Brusseau, M.L., Jim Yeh, T.C., Gerba, C.P., Harvey, R., 2005. Influence of water chemistry and travel distance on bacteriophage PRD-1 transport in a sandy aquifer. Water Res. 39, 2345–2357.

Bullo, S., Buskaran, K., Baby, R., Dorniani, D., Fakurazi, S., Hussein, M.Z., 2019. Dual drugs anticancer nanoformulation using graphene oxide-PEG as nanocarrier for protocatechuic acid and chlorogenic acid. Pharm. Res. 36, 91.

Chang, Y., Yang, S.T., Liu, J.H., Dong, E., Wang, Y., Cao, A., et al., 2011. In vitro toxicity evaluation of graphene oxide on A549 cells. Toxicol. Lett. 200, 201–210.

Chen, C., Shang, J., Zheng, X., Zhao, K., Yan, C., Sharma, P., et al., 2018a. Effect of physicochemical factors on transport and retention of graphene oxide in saturated media. Environ. Pollut. 236, 168–176.

Chen, J., Lu, T., Wang, Y., Li, J., Fu, X., Qi, Z., et al., 2019. Transport of graphene oxide nanoparticles in saturated kaolinite- and goethite-coated sand columns: effects of low-molecular-weight organic acids. Environ. Sci. Pollut. Res. 26, 24922–24932.

Chen, M., Alim, N., Zhang, Y., Xu, N., Cao, X., 2018b. Contrasting effects of biochar nanoparticles on the retention and transport of phosphorus in acidic and alkaline soils. Environ. Pollut. 239, 562–570.

Chen, M., Xu, N., Cao, X., Zhou, K., Chen, Z., Wang, Y., et al., 2015. Facilitated transport of anatase titanium dioxides nanoparticles in the presence of phosphate in saturated sands. J. Colloid Interface Sci. 451, 134–143.

Chrysikopoulos, C.V., Sotirelis, N.P., Kallithrakas-Kontos, N.G., 2017. Cotransport of graphene oxide nanoparticles and kaolinite colloids in porous media. Transport Porous Med 119, 181–204.

Dong, S., Shi, X., Gao, B., Wu, J., Sun, Y., Guo, H., et al., 2016. Retention and release of graphene oxide in structured heterogeneous porous media under saturated and unsaturated conditions. Environ. Sci. Technol. 50, 10397–10405.

Dong, S., Sun, Y., Gao, B., Shi, X., Xu, H., Wu, J., et al., 2017. Retention and transport of graphene oxide in water-saturated limestone media. Chemosphere 180, 506–512.

Dreyer, D.R., Park, S., Bielawski, C.W., Ruoff, R.S., 2010. The chemistry of graphene oxide. Chem. Soc. Rev. 39, 228–240.

Dreyer, D.R., Todd, A.D., Bielawski, C.W., 2014. Harnessing the chemistry of graphene oxide. Chem. Soc. Rev. 43, 5288–5301.

Duster, T.A., Na, C., Bolster, D., Fein, J.B., 2016. Transport of single-layered graphene oxide nanosheets through quartz and iron oxide–coated sand columns. J. Environ. Eng., 04016079.

Fan, W., Jiang, X., Lu, Y., Huo, M., Lin, S., Geng, Z., 2015a. Effects of surfactants on graphene oxide nanoparticles transport in saturated porous media. J. Environ. Sci. 35, 12–19.
Fan, W., Jiang, X., Yang, W., Geng, Z., Huo, M.X., Liu, Z., et al., 2015b. Transport of graphene oxide in saturated porous media: effect of cation composition in mixed Na-Ca electrolyte systems. Sci. Total Environ. 511, 509–515.
Feng, Y., Huynh, K.A., Xie, Z., Liu, G., Gao, S., 2019. Heteroaggregation and sedimentation of graphene oxide with hematite colloids: influence of water constituents and impact on tetracycline adsorption. Sci. Total Environ. 647, 708–715.
Feriancikova, L., Xu, S., 2012. Deposition and remobilization of graphene oxide within saturated sand packs. J. Hazard. Mater. 235–236, 194–200.
Gérard, F., 2016. Clay minerals, iron/aluminum oxides, and their contribution to phosphate sorption in soils — a myth revisited. Geoderma 262, 213–226.
Georgopouloua, M.P., Syngouna, V.I., Chrysikopoulos, C.V., 2020. Influence of graphene oxide nanoparticles on the transport and cotransport of biocolloids in saturated porous media. Colloids Surf. B 189, 110841 2020.
Guo, P., Xu, N., Li, D., Huangfu, X., Li, Z., 2018. Aggregation and transport of rutile titanium dioxide nanoparticles with montmorillonite and diatomite in the presence of phosphate in porous sand. Chemosphere 204, 327–334.
Han, P., Shen, X., Yang, H., Kim, H., Tong, M., 2013. Influence of nutrient conditions on the transport of bacteria in saturated porous media. Colloids surf. B 102, 752–758.
Jaya Seema, D.M., Saifullah, B., Selvanayagam, M., Gothai, S., Hussein, M.Z., Subbiah, S.K., et al., 2018. Designing of the anticancer nanocomposite with sustained release properties by using graphene oxide nanocarrier with phenethyl isothiocyanate as anticancer agent. Pharmaceutics 10, 109.
Jiang, Y., Yin, X., Guan, D., Jing, T., Sun, H., Wang, N., et al., 2019. Co-transport of Pb(II) and oxygen-content-controllable graphene oxide from electron-beam-irradiated graphite in saturated porous media. J. Hazard. Mater. 375, 297–304.
Jiang, Y., Zhang, X., Yin, X., Sun, H., Wang, N., 2018. Graphene oxide-facilitated transport of Pb^{2+} and Cd^{2+} in saturated porous media. Sci. Total Environ. 631–632, 369–376.
Katzourakis, V.E., Chrysikopoulos, C.V., 2018. Impact of spatially variable collision efficiency on the transport of biocolloids in geochemically heterogeneous porous media. Water Resour. Res. 54, 3841–3862.
Kosmulski, M., 2004. pH-dependent surface charging and points of zero charge II. Update. J. Colloid Interface Sci. 275, 214–224.
Lanphere, J.D., Luth, C.J., Walker, S.L., 2013. Effects of solution chemistry on the transport of graphene oxide in saturated porous media. Environ. Sci. Technol. 47, 4255–4261.
Lanphere, J.D., Rogers, B., Luth, C., Bolster, C.H., Walker, S.L., 2014. Stability and transport of graphene oxide nanoparticles in groundwater and surface water. Environ. Eng. Sci. 31, 350–359.
Lecoanet, H.F., Bottero, J.Y., Wiesner, M.R., 2004. Laboratory assessment of the mobility of nanomaterials in porous media. Environ. Sci. Technol. 38, 5164–5169.
Leij, F.J., Bradford, S.A., Sciortino, A., 2016. Analytic solutions for colloid transport with time - and depth-dependent retention in porous media. J. Contam. Hydrol. 195, 40–51.
Li, J., Chen, J., Lu, T., Wang, Y., Zhang, H., Shang, Z., et al., 2019. Effects of low-molecular weight organic acids on the transport of graphene oxide nanoparticles in saturated sand columns. Sci. Total Environ. 666, 94–102.
Li, L., Schuster, M., 2014. Influence of phosphate and solution pH on the mobility of ZnO nanoparticles in saturated sand. Sci. Total Environ. 472, 971–978.
Li, M., Liu, J., Xu, Y., Qian, G., 2016. Phosphate adsorption on metal oxides and metal hydroxides: a comparative review. Environ. Rev. 24, 319–332.
Liang, Y., Bradford, S.A., Simunek, J., Heggen, M., Vereecken, H., Klumpp, E., 2013. Retention and remobilization of stabilized silver nanoparticles in an undisturbed loamy sand soil. Environ. Sci. Technol. 47, 12229–12237.
Lin, J., Zhan, Y., Wang, H., Chu, M., Wang, C., He, Y., et al., 2017. Effect of calcium ion on phosphate adsorption onto hydrous zirconium oxide. Chem. Eng. J. 309, 118–129.
Liu, C., Xu, N., Feng, G., Zhou, D., Cheng, X., Li, Z., 2017. Hydrochars and phosphate enhancing the transport of nanoparticle silica in saturated sands. Chemosphere 189, 213–223.
Liu, X., Chen, K.L., 2016. Aggregation and interactions of chemical mechanical planarization nanoparticles with model biological membranes: role of phosphate adsorption. Environ. Sci. Nano 3, 146–156.
Liu, X., Li, M., Liu, F., He, L., Tong, M., 2019. Cotransport of graphene oxides/reduced graphene oxides with BPA in both bare and iron oxides coated quartz sand. Sci. China Technol. Sci. 62, 1896–1906.
Liu, L., Gao, B., Wu, L., Morales, V.L., Yang, L., Zhou, Z., et al., 2013. Deposition and transport of graphene oxide in saturated and unsaturated porous media. Chem. Eng. J. 229, 444–449.
Lu, X., Lu, T., Zhang, H., Shang, Z., Chen, J., Wang, Y., et al., 2019. Effects of solution chemistry on the attachment of graphene oxide onto clay minerals. Environ. Sci.: Processes Impacts 21, 506–513.
Lucia, F., Xu, S.P., 2012. Deposition and remobilization of graphene oxide within saturated sand packs. J. Hazard. Mater. 235–236, 194–200.
Millero, F., Huang, F., Zhu, X.R., Liu, X.W., Zhang, J.Z., 2001. Adsorption and desorption of phosphate on calcite and aragonite in seawater. Aquat. Geochem 7, 33–56.
Mitropoulou, P.N., Syngouna, V.I., Chrysikopoulos, C.V., 2013. Transport of colloids in unsaturated packed columns: role of ionic strength and sand grain size. Chem. Eng. J. 232, 237–248.
Morales, V.L., Gao, B., Steenhuis, T.S., 2009. Grain surface-roughness effects on colloidal retention in the vadose zone. Vadose Zone J. 8, 11–20.
Stumm, W., Morgan, J.J., 1981. Aquatic Chemistry: an Introduction Emphasizing Chemical Equilibria in Natural Waters. John Wiley Book..
Mu, Y., Ai, Z., Zhang, L., 2017. Phosphate shifted oxygen reduction pathway on $Fe@Fe_2O_3$ core-shell nanowires for enhanced reactive oxygen species generation and aerobic 4-chlorophenol degradation. Environ. Sci. Technol. 51, 8101–8109.
Murashov, V.V., Leszczynski, J., 1999. Adsorption of the phosphate groups on silica hydroxyls: an ab initio study. J. Phys. Chem. A 103, 1228–1238.
Nowack, B., Stone, A.T., 2006. Competitive adsorption of phosphate and phosphonates onto goethite. Water Res. 40, 2201–2209.
Park, S.J., Lee, C.G., Kim, S.B., 2009. The role of phosphate in bacterial interaction with iron-coated surfaces. Colloid Surf. B 68, 79–82.
Persson, P., Nilsson, N., Sjoberg, S., 1996. Structure and bonding of orthophosphate ions at the iron oxide–aqueous interface. J. Colloid Interface Sci. 177, 263–275.
Qi, Z., Du, T., Ma, P., Liu, F., Chen, W., 2019. Transport of graphene oxide in saturated quartz sand containing iron oxides. Sci. Total Environ. 657, 1450–1459.
Qi, Z., Hou, L., Zhu, D., Ji, R., Chen, W., 2014a. Enhanced transport of phenanthrene and 1-naphthol by colloidal graphene oxide nanoparticles in saturated soil. Environ. Sci. Technol. 48, 10136–10144.
Qi, Z., Zhang, L., Chen, W., 2014b. Transport of graphene oxide nanoparticles in saturated sandy soil. Environ. Sci. Proc. Impacts 16, 2268–2277.

Qi, Z., Zhang, L., Wang, F., Hou, L., Chen, W., 2014c. Factors controlling transport of graphene oxide nanoparticles in saturated sand columns. Environ. Toxicol. Chem. 33, 998–1004.
Qin, X., Liu, F., Wang, G., 2012. Fractionation and kinetic processes of humic acid upon adsorption on colloidal hematite in aqueous solution with phosphate. Chem. Eng. J. 209, 458–463.
Qin, X., Liu, F., Wang, G., Weng, L., Li, L., 2014. Adsorption of levofloxacin onto goethite: effects of pH, calcium and phosphate. Colloids surf. B 116, 591–596.
Ramazanpour Esfahani, A., Batelaan, O., Hutson, J.L., Fallowfield, H.J., 2020. Effect of bacteria and virus on transport and retention of graphene oxide nanoparticles in natural limestone sediments. Chemosphere 248, 125929.
Ren, X., Wu, Q., Xu, H., Shao, D., Tan, X., Shi, W., et al., 2016. New insight into GO, cadmium(II), phosphate interaction and its role in GO colloidal behavior. Environ. Sci. Technol. 50, 9361–9369.
Rietra, R.P.J.J., Hiemstra, T., Van Riemsdijk, W.H., 2001. Interaction between calcium and phosphate adsorption on goethite. Environ. Sci. Technol. 36, 3369–3374.
Shen, C., Li, B., Wang, C., Huang, Y., Jin, Y., 2011. Surface roughness effect on deposition of nano- and micro-sized colloids in saturated columns at different solution ionic strengths. Vadose Zone J. 10, 1071–1081.
Shen, M., Hai, X., Shang, Y., Zheng, C., Li, P., Li, Y., et al., 2019. Insights into aggregation and transport of graphene oxide in aqueous and saturated porous media: complex effects of cations with different molecular weight fractionated natural organic matter. Sci. Total Environ. 656, 843–851.
Stahl, R.S., James, B.R., 1991. Zinc sorption by iron-oxide-coated sand as a function of pH. Soil Sci. Soc. Am. J. 55, 1291–1294.
Sun, K., Dong, S., Sun, Y., Gao, B., Du, W., Xu, H., et al., 2018. Graphene oxide-facilitated transport of levofloxacin and ciprofloxacin in saturated and unsaturated porous media. J. Hazard. Mater. 348, 92–99.
Sun, Y., Gao, B., Bradford, S.A., Wu, L., Chen, H., Shi, X., et al., 2015. Transport, retention, and size perturbation of graphene oxide in saturated porous media: effects of input concentration and grain size. Water Res. 68, 24–33.
Syngouna, V.I., Giannadakis, G.I., Chrysikopoulos, C.V., 2020. Interaction of graphene oxide nanoparticles with quartz sand and montmorillonite colloids. Environ. Technol. 41, 1127–1138.
Tejedor-Tejedor, M.I., Anderson, M.A., 1990. The protonation of phosphate on the surface of goethite as studied by CIR-FTIR and electrophoretic mobility. Langmuir 63, 602–611.
Tofan-Lazar, J., Al-Abadleh, H.A., 2012. Kinetic ATR-FTIR studies on phosphate adsorption on iron (oxyhydr)oxides in the absence and presence of surface arsenic: molecular-level insights into the ligand exchange mechanism. J. Phys. Chem. A 116, 10143–10149.
Tufenkji, N., Elimelech, M., 2004. Deviation from the classical colloid filtration theory in the presence of repulsive DLVO interactions. Langmuir 20, 10818–10828.
Tufenkji, N., Elimelech, M., 2005. Breakdown of colloid filtration theory: role of the secondary energy minimum and surface charge heterogeneities. Langmuir 21, 841–852.
Wang, D., Bradford, S.A., Harvey, R.W., Gao, B., Cang, L., Zhou, D., 2012. Humic acid facilitates the transport of ARS-labeled hydroxyapatite nanoparticles in iron oxyhydroxide-coated Sand. Environ. Sci. Technol. 46 (5), 2738–2745.
Wang, K., Ruan, J., Song, H., Zhang, J., Wo, Y., Guo, S., et al., 2011a. Biocompatibility of graphene oxide. Nanoscale Res. Lett. 6, 8.
Wang, D., Shen, C., Jin, Y., Su, C., Chu, L., Zhou, D., 2017a. Role of solution chemistry in the retention and release of graphene oxide nanomaterials in uncoated and iron oxide-coated sand. Sci. Total Environ. 579, 776–785.
Wang, G., Wang, B., Park, J., Yang, J., Shen, X., Yao, J., 2009. Synthesis of enhanced hydrophilic and hydrophobic graphene oxide nanosheets by a solvothermal method. Carbon N Y 47, 68–72.
Wang, H., Zhu, J., Fu, Q., Hong, C., Hu, H., Violante, A., 2016. Phosphate adsorption on uncoated and humic acid-coated iron oxides. J. Soil Sediment 16, 1911–1920.
Wang, M., Gao, B., Tang, D., Sun, H., Yin, X., Yu, C., 2017b. Effects of temperature on graphene oxide deposition and transport in saturated porous media. J. Hazard. Mater. 331, 28–35.
Wang, M., Song, Y., Zhang, H., Lu, T., Chen, W., Li, W., et al., 2021. Insights into the mutual promotion effect of graphene oxide nanoparticles and tetracycline on their transport in saturated porous media. Environ. Pollut. 268, 115730.
Wang, L., Xu, S., Li, J., 2011b. Effects of phosphate on the transport of *Escherichia coli* O157:H7 in saturated quartz sand. Environ. Sci. Technol 45, 9566–9573.
Wang, M., Yu, C., Tang, D., Chen, J., Gao, B., 2019. Effects of surfactant and electrolyte concentrations, cation valence, and temperature on graphene oxide retention and transport in saturated porous media. Water Air Soil Pollut 230, 21.
Weng, L., Riemsdijk, W.H.V., Hiemstra, T., 2008. Humic nanoparticles at the oxide-water interface: interactions with phosphate ion adsorption. Environ. Sci. Technol. 42, 8747–8752.
Xia, T., Fortner, J.D., Zhu, D., Qi, Z., Chen, W., 2015. Transport of sulfide-reduced graphene oxide in saturated quartz sand: cation-dependent retention mechanisms. Environ. Sci. Technol. 49, 11468–11475.
Xia, T., Lin, Y., Guo, X., Li, S., Cui, J., Ping, H., et al., 2019a. Co-transport of graphene oxide and titanium dioxide nanoparticles in saturated quartz sand: influences of solution pH and metal ions. Environ. Pollut. 251, 723–730.
Xia, T., Ma, P., Qi, Y., Zhu, L., Qi, Z., Chen, W., 2019b. Transport and retention of reduced graphene oxide materials in saturated porous media: synergistic effects of enhanced attachment and particle aggregation. Environ. Pollut. 247, 383–391.
Xia, T., Qi, Y., Liu, J., Qi, Z., Chen, W., Wiesner, M.R., 2017. Cation-inhibited transport of graphene oxide nanomaterials in saturated porous media: the Hofmeister effects. Environ. Sci. Technol. 51, 828–837.
Xu, H., Hu, J., Ren, X., Li, G., 2016a. Macroscopic and microscopic insight into the mutual effects of europium(III) and phosphate on their interaction with graphene oxide. RSC Adv 6, 85046–85057.
Xu, C.Y., Xu, R.K., Li, J.Y., Deng, K.Y., 2016b. Phosphate-induced aggregation kinetics of hematite and goethite nanoparticles. J. Soil Sediment 17, 352–363.
Xu, N., Cheng, X., Wang, D., Xu, X., Huangfu, X., Li, Z., 2018. Effects of Escherichia coli and phosphate on the transport of titanium dioxide nanoparticles in heterogeneous porous media. Water Res 146, 264–274.
Yang, H., Kim, H., Tong, M., 2012. Influence of humic acid on the transport behavior of bacteria in quartz sand. Colloids surf. B 91, 122–129.
Yin, X., Jiang, Y., Tan, Y., Meng, X., Sun, H., Wang, N., 2019. Co-transport of graphene oxide and heavy metal ions in surface-modified porous media. Chemosphere 218, 1–13.
Zhang, H., Lu, T., Shang, Z., Li, Y., He, J., Liu, S., et al., 2020. Transport of Cd^{2+} through saturated porous media: insight into the effects of low-molecular-weight organic acids. Water Res. 168, 115182.
Zhang, J., Xie, X., Meng, X., Li, Y., Zhu, W., 2019. Release and transport of Pb(II) adsorbed on graphene oxide under alkaline conditions in a saturated sand column. J. Hazard. Mater. 377, 357–364.
Zhao, C., Pei, S., Ma, J., Song, Z., Xia, H., Song, X., et al., 2020. Influence of graphene oxide nanosheets on the cotransport of cu-tetracycline multi-pollutants in saturated porous media. Environ. Sci. Pollut. Res. 27, 10846–10856.

Zhao, J., Wang, Z., White, J.C., Xing, B., 2014. Graphene in the aquatic environment: adsorption, dispersion, toxicity and transformation. Environ. Sci. Technol. 48, 9995–10009.
Zhang, C., Yan, A., Wang, G., Jin, C., Chen, Y., Shen, C., 2018. Impact of flow velocity on transport of graphene oxide nanoparticles in saturated porous media. Vadose Zone J 17, 180019.
Zhao, K., Chen, C., Cheng, T., Shang, J., 2019. Graphene oxide-facilitated uranium transport and release in saturated medium: effect of ionic strength and medium structure. Environ. Pollut. 247, 668–677.
Zhou, D.D., Jiang, X.H., Lu, Y., Fan, W., Huo, M.X., Crittenden, J.C., 2016. Cotransport of graphene oxide and Cu(II) through saturated porous media. Sci. Total Environ. 550, 717–726.
Zhuang, J., Jin, Y., 2008. Interactions between viruses and goethite during saturated flow: effects of solution pH, carbonate, and phosphate. J. Contam. Hydrol. 98, 15–21.